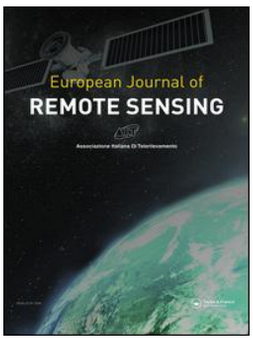

European Journal of Remote Sensing

ISSN: (Print) 2279-7254 (Online) Journal homepage: http://www.tandfonline.com/loi/tejr20

Empirical line model for the atmospheric correction of sentinel-2A MSI images in the Caribbean Islands

Alexander Ariza, Marina Robredo Irizar & Steven Bayer

To cite this article: Alexander Ariza, Marina Robredo Irizar & Steven Bayer (2018) Empirical line model for the atmospheric correction of sentinel-2A MSI images in the Caribbean Islands, European Journal of Remote Sensing, 51:1, 765-776, DOI: 10.1080/22797254.2018.1482732

To link to this article: https://doi.org/10.1080/22797254.2018.1482732

Published online: 19 Jul 2018.

EUROPEAN JOURNAL OF REMOTE SENSING
2018, VOL. 51, NO. 1, 765–776
https://doi.org/10.1080/22797254.2018.1482732

Taylor & Francis
Taylor & Francis Group

Empirical line model for the atmospheric correction of sentinel-2A MSI images in the Caribbean Islands

Alexander Ariza[a], Marina Robredo Irizar[b] and Steven Bayer[c]

[a]Research and Investigation Centre, CIAF, Instituto Geográfico Agustín Codazzi – IGAC, Bogotá, Colombia; [b]Civil Engineering and Geoinformatics, Beuth Houchschule Fur Technik, University of Applicate Sciences, Berlin, Germany; [c]Department for Sensor Concepts and Applications, Institut Optische Sensorsysteme, DLR, Berlin, Germany

ABSTRACT

An Empirical Line Model (ELM) was tested to correct Sentinel-2A (MSI) images acquired in the tropical archipelago of San Andrés, Colombia. This approach uses a linear regression to model the relationship between the average ground reflectance and radiance on bands 2, 3, 4, and 8, for 32 spectrally homogeneous targets. The model was validated from eight targets measured on different land-covers trough the estimated coefficient of determination R^2. The result of the prediction equations observed was high, with a value of R^2:0.91 performed at the 0.01 level of significance for the four wavebands, against the R^2:0.77 of SEN2COR and R^2:0.81 of ATCOR Correction Models. Complementary, a quantitative approach was proposed to determine the suitability of the ELM, based on the spectral response on six land-covers types for every band after correction. A separability index (M) was used from a set of independent targets to estimate the effectiveness of spectral classification of land-covers. The more evident results of the correction are on the vegetation cover in the NIR band (785–900 nm), where the ELM has 55% and 58% more separability than the SEN2COR and ATCOR models, respectively. Additionally, the absolute difference between the Top-of-Atmosphere (TOA) and Bottom-of-Atmosphere (BOA) images was calculated, finding the highest differences in the NIR band with 0.094 in the L1C-TOA reflectance image, and 0.013 in the ELM-BOA image. Finally, a sensitivity analysis on the Normalized Difference Vegetation Index (NDVI) to estimate the performance of the spectral response of ELM on vegetation cover was employed.

ARTICLE HISTORY
Received 8 November 2017
Revised 16 May 2018
Accepted 28 May 2018

KEYWORDS
ELM; Sentinel-2A; SEN2COR; ATCOR; Caribbean Islands; atmospheric correction

Introduction

To collect remote sensed data of lasting quantitative value, it is necessary to calibrate them to physical units such as reflectance. However, this information is affected by sensor characteristics, illumination geometry and atmospheric conditions, and, therefore, it is commonly expressed in arbitrary units such as digital number (DN) (Vanonckelen, Lhermitte, & Van Rompaey, 2013). In the case of passive remote sensing systems, only the naturally occurring radiation is used, which can be solar or thermal radiation (due to surface temperature). Radiation measured at the satellite sensor or Top-of-Atmosphere (TOA) has passed through the Earth's atmosphere twice: on the way from the sun to the earth's surface and from the earth's surface to the sensor.

The effects of atmospheric scattering and absorption must be removed from satellite remotely sensed data if such images are to be used quantitatively and transformed into reflectance values of the ground surface or Bottom-of-Atmosphere (BOA), which are particularly important for marine environment study due to the proportionately greater contribution to at-sensor received radiance over water targets (Goyens, Jamet, & Schroeder, 2013; Werdell, Franz, & Bailey, 2010). There are a number of methods to account for the influence of illumination and the atmosphere on sensor-recorded data (Table 1 summarizes the most commonly used correction methods), and the performances of which have been compared by several authors (Ferrier & Trahair, 1995; Minomura, Kuze, & Takeuchi, 2001; Vanonckelen et al., 2013)

The resulting atmospheric correction algorithms from these models are mostly designed for remote sensing of land surfaces. However, these algorithms are not directly applicable for spectral remote sensing of ocean color, because ocean surfaces are much darker than land surfaces and the air/water interface is not a Lambertian accurate modeling of atmospheric absorption and scattering effects, in addition to the specular ocean surface reflection effects, and so there is a need to find other solutions. On the other hand, and although radiative transfer models often produce better results than other methods, they require measurements or assumed values of atmospheric variables at the time of data acquisition that may be difficult to obtain, especially when dealing with historical datasets or the inaccessible zones. Ocean zones leaving reflectance is the reflectance resulting from

CONTACT Alexander Ariza aariza@ucm.edu.co Instituto Geográfico Agustín Codazzi – IGAC, Bogotá, Colombia

Table 1. Main models of atmospheric correction applied to remote sensing.

Model	Reference	Description
DOS	(Chávez, 1996)	The dark object subtraction method
Empirical line	Smith & Milton, 1999	Empirical line method by correlation of endmembers
LOWTRAN-7	(Kneizys et al., 1988)	Low resolution atmospheric transmission model
ATCOR	(Richter, 1996)	Atmospheric and topographic correction model
FLAASH	(Matthew et al., 2003)	Atmospheric correction tool on MODTRAN4 radiation transfer code.
6S	(Sriwongsitanon, Surakit, & Thianpopirug, 2011)	The second simulation of a satellite signal in the solar spectrum
Inverse technique	(Gilabert, Conese, & Maselli, 1994)	An inversion algorithm based on a Simplified radiative transfer model
SMAC	(Rahman & Dedieu, 1994)	Simplified method for atmospheric correction
MODTRAN	(Berk et al., 1998)	Moderate resolution atmospheric transmission model
Look-up tables	(Liang & Fang, 2004)	Neural network algorithm for estimating water vapor
Transmittance functions	(Kobayashi & Sanga-Ngoie, 2008)	Part of the integrated radiometric correction
RTC's, and DOS	(Moran, Jackson, Slater, & Teillet, 1992)	Radiative transfer codes (RTCs) with simulated atmospheres, image-based procedures and dark-object subtraction (DOS)
SEN2COR	(Müller-Wilm, 2016)	A processor for Sentinel-2 Level 2A atmospheric correction, based in libRadtran.

scattering by water bodies, excluding contributions from specular reflection at the air/water interface. If we neglect the interactions between atmospheric gaseous absorption and molecular and aerosol scattering above water surfaces, the measured apparent reflectance,ρ_{obs}, can be expressed as Equation (1) (Gao, Montes, Davis, & Goetz, 2009):

$$\rho_{obs} = \left[\rho_{atm+sfc} + \rho_w t_d t_u / \left(1 - s\rho_w\right)\right] T_g \qquad (1)$$

where t_d is the downward scattering transmittance, t_u the upward scattering transmittance, s the spherical albedo of the atmosphere, and T_g the total gaseous transmittance in the Sun-surface-sensor path, $\rho_{atm+sfc}$ is the reflectance resulting from scattering by the atmosphere and specular reflection by ocean surface aspects, and ρ_w is the water leaving reflectance.

In the 1980s, several scene-based empirical approaches were developed to remove atmospheric effects from spectral imaging data in order to obtain relative surface reflectance spectra; in addition, atmospheric absorption and scattering effects were removed by these empirical models. This process normally involves transforming the spectral data from radiance, *L (W m-2 μm-1 sr-1)*, to scaled percent surface reflectance or BOA. This transformation allows the spectral reflectance data, obtained by the remote sensor (often referred to as endmembers), to be quantitatively compared with spectral reflectance data obtained on the ground using a handheld spectroradiometer captured for alternate dates or times. The use of empirical relationships to calibrate remote sensed data has been reported by many authors (Hadley, Garcia-Quijano, Jensen, & Tullis, 2005; Karpouzli & Malthus, 2003), but little, if any, information is given on the selection and characterization of field targets. Furthermore, some studies have used a few calibration targets without validation targets to assess the error in the empirical relationships. Insufficient knowledge of the calibration procedure, the local conditions, and the spectral properties of the proposed calibration targets can lead to erroneous results (Hadley et al., 2005).

The aim of this paper is to evaluate the precision and efficiency of an empirical line method (ELM) of atmospheric correction for Sentinel-2A images of Caribbean zones and, in this process, to identify some of the limitations and outline the requirements of suitable calibration targets. The three atmospheric correction models tested were the ELM method, the Atmospheric Correction ATCOR (Ver.3) model, and the SEN2COR-based model. This research also assessed the effect that the atmospheric correction has on the spectral separability (M) of each of the main land-covers. Finally, we evaluated the effect of the atmospheric correction TOA and BOA, on the spectral index NDVI, through absolute differences on band ratios.

Materials and methods

Study area and data acquisition

The Colombian tropical island of San Andrés is located in the West Caribbean Sea, 620 km northwest of Cartagena (Colombia coast) and about 190 km east of the Nicaraguan coast, at the geographic coordinates of 12° 33′N and 81° 43′W in the archipelago of San Andrés y Providencia. The total area of the archipelago is about 180,000 km^2, of which about 1% is land mass and consists mainly of seven islands, plus small cays, atolls, sandbanks (all of which are mostly uninhabited) and reefs. The island of San Andrés, the most populated island in the archipelago, has a north-south extension of 12 km and an east-west extension of maximum 4 km (Figure 1). It is located in the tip of a sunken volcano whose base is more than 1000 m below sea level, and various reefs have formed around the island. It is also noteworthy to mention that three subareas of a total of 65 018 km2 of the archipelago have been validated as protected marine area since 2005, and in November 2000, the archipelago was declared as the "Seaflower Biosphere Reserve."

The Sentinel-2A (S2-A) satellite image was acquired on 16 August 2016. The S2-A is part of the earth

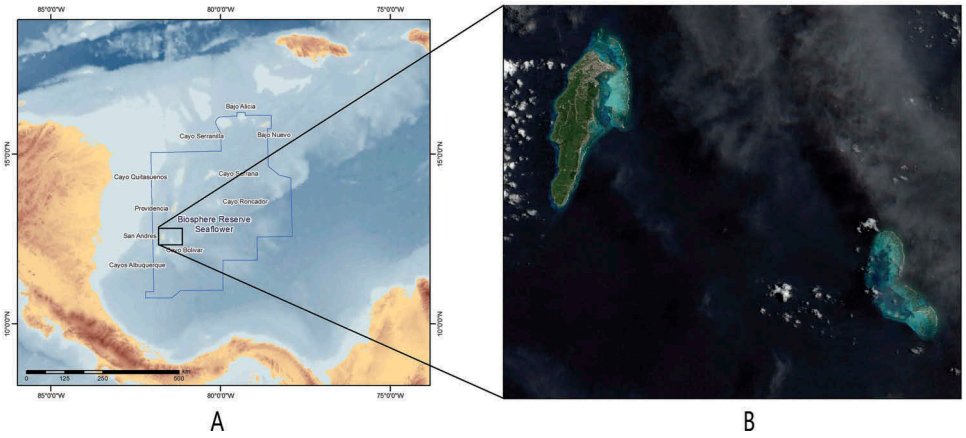

Figure 1. (A) Archipelago of San Andres and Providence — Colombia. (B) San Andres Island (left) and East-west Cay (right), composed of red, green, and blue.

observation mission developed by the European Space Agency and was launched on 23 June 2015 (Drusch et al., 2012). The mission is based on a satellite constellation deployed in polar sun-synchronous orbit, providing multispectral data with a five-day revisit frequency and a wide field of view (290 km), carrying a single multi-spectral instrument (MSI) with 13 spectral bands, which use the push-broom concept. The spatial resolution of Sentinel-2A varies between 10 and 60 m.

In situ spectroradiometer data

All observations were made according to the CIAF[1] methodology for field spectroradiometry, under the protocol of the USGS Spectroscopy Laboratory (USGS, 2017). *In situ* data were collected at each of the 24 sample site locations with two spectroradiometers: the first one is a "fieldspect-4" built by Analytical Spectral Devices (ASD) that covered the wavelength range of 350–2500 nm at 1 nm intervals and has a field-of-view (FOV) of 25 degrees. The spectra were acquired from a height of 1.5 m above the ground. The second spectroradiometer is a HR2000 of Ocean Optics, with a wavelength range of 350–900 nm and a FOV of 25 degrees (Figure 2).

Individual target spectra were converted to reflectance with the use of a Spectralon white calibration panel, where every measurement is derived from an average of the collection of 10 spectra at each target. First, a reference spectrum was collected from the Spectralon panel at ground level, and each endmember was taken with the criteria of spectral and spatial uniformity, in order to avoid adjacent noise; the final spectra were again a reference shot collected from the Spectralon panel at ground level. The measurements were taken on the same day of the satellite passage, over a maximum time interval of ±3 h to capture the image. Post-processing of the spectra consisted of several steps, from the calculation of the measurements average, to the transformation of raw data into ND of the endmember in percentage values of reflectance. Finally, eight calibration reference endmembers were obtained at the target point locations, and then these measurements were compiled into a field spectral library.

Methodology

The flowchart of the methodology presented in Figure 3 shows how our workflow is composed: imagery pre-processing, implementation of the atmospheric corrections models (ELM, SEN2COR, and ATCOR), separability analysis of land-cover types and its accuracy assessment.

After pre-processing of the S2-A MSI data, the image was atmospherically corrected to ground reflectance (BOA) in order to check the accuracy of the correction, which used 32 targets for calibration and 8 for validation (for a 40 total targets available), for four types on land-covers from the total six defined (vegetation, coral rocks, soil, asphalt, sand, and deep water); this is grounded in a 80–20 percent (calibration and validation respectively) distribution of the targets from a Pareto principle basis. The absolute differences between the current value (field data) and the calculated value (ELM) are then calculated. In this study, we calculated the Root Mean Square Error (RMSE) and the determination coefficient R-squared (R^2), as a measure of accuracy. The separability of the models was calculated to determine its discrimination capability in different cover areas, through a comparative analysis in the visible (VIS) and near-infrared (NIR) spectral regions (B2, B3, B4, and B8). Thirdly, a sensitivity analysis was conducted in order to determine the suitability of the ELM model approach, based on the spectral response of every band after correction; for this, a variety of

[1]*Research and Investigation Centre on Geographic Information of the Geographic Institute Agustín Codazzi of Colombia.*

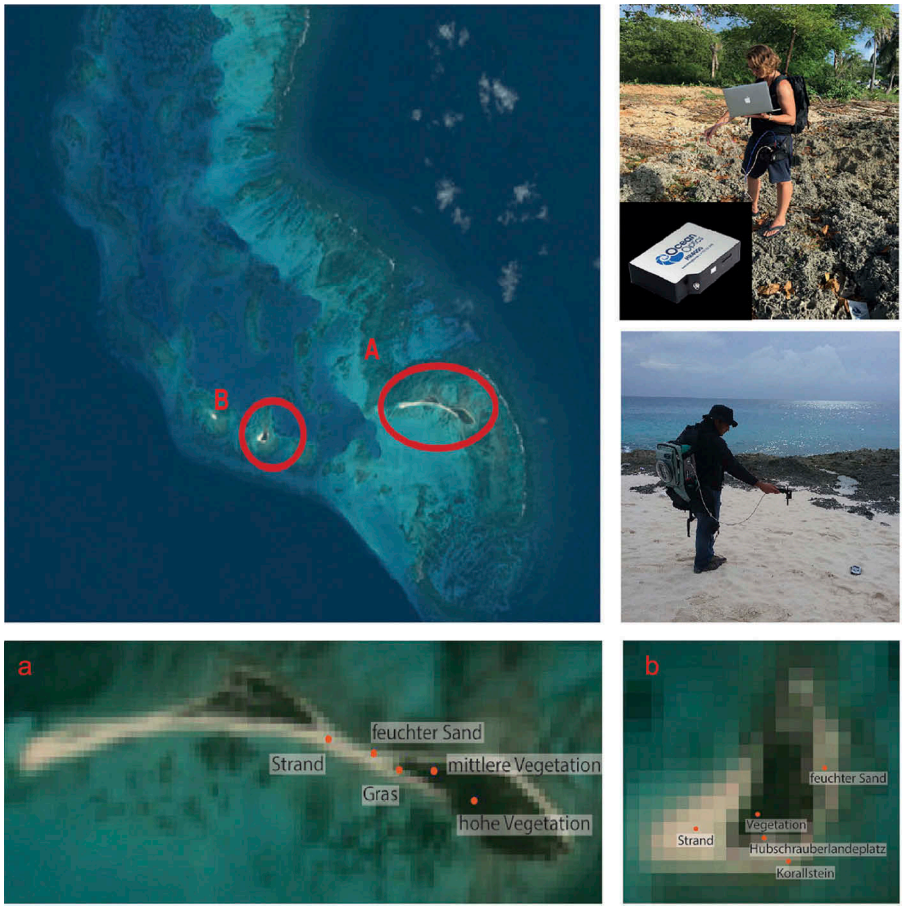

Figure 2. Spectral measures in field on East-west Cay, (A) Bolivar Cay, (B) Virgen Island.

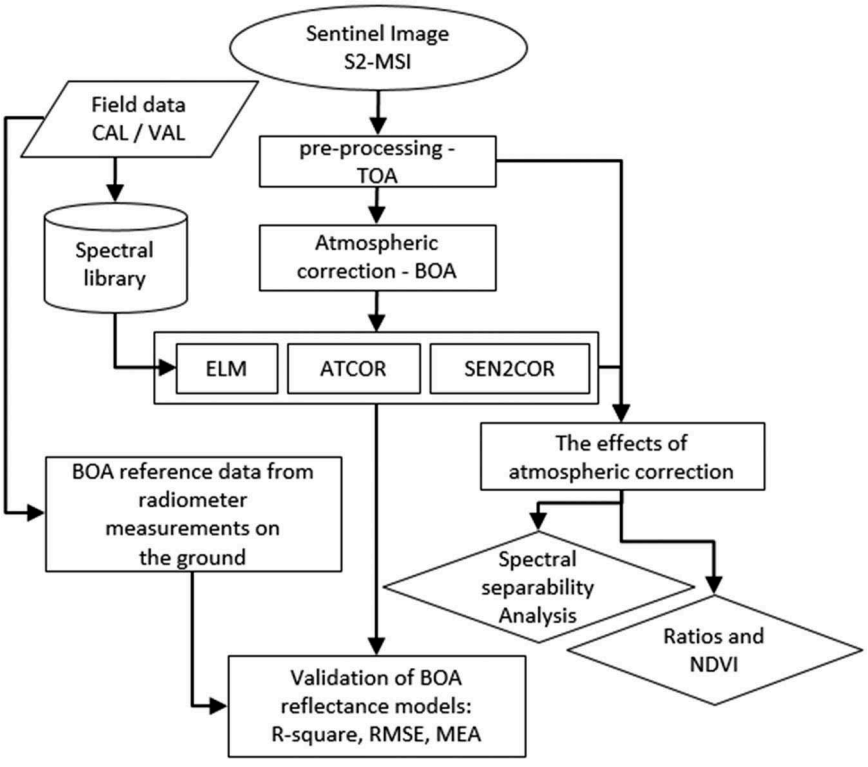

Figure 3. Flowchart of the methodology.

covers were selected using a set of independent targets; a separability index (M) was then used to estimate the effectiveness in the discrimination of land-covers; and finally, we measured the differences of the relative error on every NDVI obtained after the atmospheric correction from every model.

Imagery preprocessing

S2-A captured an image over the San Andrés and Providencia archipelago on 16 August 2016 at 15:56 (UTC-6). This image was downloaded from the ESA DataHUB server (https://scihub.copernicus.eu/dhus/) as a Level 1C product, which means that it is already geometrically corrected from a rational function computed from ground control points (GCP) and projected to Universal Transverse Mercator coordinate system (UTM, Zone 17 North, World Geodetic System1984). To facilitate spectral analysis between endmembers, on-field targets and the S2-A image were co-registered in the island zones, having a co-registration error (RMSE) of 8.2 m, using the 40 targets as GCP, second-order polynomial transformation and nearest neighbor resampling.

We conducted atmospheric correction procedures on reprocessed L1C (TOA – Top of Atmosphere Reflectance data) (processing baseline: 02.01) using three different algorithms: ELM, Empirical Line Model, (Hadley et al., 2005; Karpouzli & Malthus, 2003), SEN2COR (Version 2.2.1), (Müller-Wilm, 2016), and ATCOR, Version 3, (Richter, 1996).

The empirical line model

Various implementations of the ELM method have been used with varying degrees of success (Smith et al., 1999). The simplest approach is to use a single calibration target and assume that surfaces with zero reflectance will produce zero radiance at the sensor and that there is a linear relationship between radiance and reflectance, although it is more common to use several calibration targets with a large spectral contrast between them, thus, removing the effect of atmospheric radiance. This method forces the remote sensing imaging spectrometer data to match with *in situ* reflectance spectra by a linear regression fit. Equation (2) describes mathematically this methodology:

$$DN_b = \rho(\lambda)A_b + B_b \tag{2}$$

where DN_b is the digital output value for a given pixel in band b, $\rho(\lambda)$ equals the reflectance of the target covers within the IFOV (instant field-of-view) at a specific wavelength (λ), A_b is the multiplicative value affecting the DN, and B_b is the additive value The multiplicative term is concerned with transmittance and instrumental factors, and the additive value deals primarily with atmospheric path radiance and instrumental offset. The implementation of the ELM provides the gain and offset values, through a first-order equation. To apply this method, two or more homogeneous (both spatially and spectrally) areas with different albedos (from the brightest to the darkest target) are needed. The gain and offset values are derived using an ordinary least squares regression fitting method Smith & Milton, 1999. The image DN and reflectance data are equated on a band-by-band basis (i.e., not pixel-by pixel) using a linear regression, thus removing the solar irradiance and the atmospheric path radiance (Hadley et al., 2005).

On the other hand, atmospheric correction models have certain limitations in Tropical and Caribbean oceanic zones, like the effects of the Aerosol Optical Thickness (AOT) — an important factor for the marine environment due to the proportionally greater contribution of water — that alters the values of real reflectance of the earth's surface (BOA) (Gao et al., 2009; Goyens et al., 2013; Rouquié et al., 2017; Werdell et al., 2010). For this reason, we have used the ELM in order to validate the results obtained by the most commonly used correction models so far (SEN2COR, ATCOR), and thus, to be able to estimate the differences in Sentinel-2A images by the implementation of the atmospheric correction models, in relation to the spectral measurements taken at the ground level.

ATCOR

The Sentinel images were atmospherically corrected using the ATCOR algorithm embedded into the software ERDAS IMAGINE (https://www.geosystems.de), in order to take into account the variations in solar illumination conditions, the atmospheric scattering and absorption. This model is a version of a large database containing results of radiative transfer calculations based on the MODTRAN-4 code, allowing the atmospheric corrections for the adjacency effect that additionally includes a correction of topographical effects (Richter, 1996).

With the ATCOR Workflow for Imagine software, the Sentinel-2 data were also corrected. The output file is provided on a layer stack of the bands 2, 3, 4, and 8 (B, G, R, and NIR). The geometric resolution of the image output file is 10 m in this case. Furthermore, different files, such as DDV map, Haze_Cloud_Water_Land map haze_Levels, AOT, Water Vapor (only in 13-band mode), Cloud_Probability, Snow/Ice_Probability (only in 13-band mode), and Water_Probability output are included into the model, just like haze distances. This process was used to obtain optimum reflectance values with the following settings:

- Dehaze mode: standard
- Use cirrus band if available
- Dehaze Area: land and water Pixels
- Interpolation: bilinear
- Watervapor: tropical
- Aerosol type: maritime
- Visibility mode: variable
- Visibility: default (23 km)

Table 2. Overview of the atmospheric and aerosol models in the current version ATCOR 2/3 (Schläpfer & Richter, 2017), reworked.

Atmosphere model	Pressure [mbar]	Water vapor column [g * cm-2]	Temperature [°C]	rel. Humidity [%]
Dry	1013	0,41	26,4	7,5
Fall/spring	1013	1,14	10,0	56
Midlatitude summer	1013	2,92	21,0	76
Midlatitude winter	1013	0,85	−1,0	77
Mubarctic summer	1013	2,08	14,0	75
Tropical	1013	4,11	26,4	75
US Standard	1013	1,42	46	46

- Adjacency: default (1 km).

The following table gives a general description of the different parameters for ATCOR model (Table 2).

SEN2COR

SEN2COR is an image processor for Sentinel-2 Level 2A product generation and formatting; it performs the atmospheric, terrain, and cirrus correction of TOA Level 1C input data. The settings to the atmospheric correction were adjusted in the Gipp-file, where the aerosol type was set to maritime, and the average width to summer, ozone content was the setting to the default value of 331 DU, and the water vapor content is obtained from band 9 (940 nm) calculation, and finally, the visibility update mode has been set to "variable."

After that, the Python application SEN2COR can be directly switched from the command line to the atmospheric correction to be started. Alternatively, SEN2COR can also be processed using SNAP software.

Prior to atmospheric correction, SEN2COR classifies the scene roughly into cloud and land-cover types. The atmospheric correction is based on 24 look-up table sets modelled with libRadtran (Müller-Wilm, 2016). SEN2COR applied a dense, dark vegetation approach to determine AOT using bands B12 (2190 nm), B04 (665 nm) and B03 (560 nm). For assessing water vapor column height, the bands B8a (865 nm) and B09 (945 nm) were used. The AOT card represents a constant AOT value of 0.114, which points to a clear sky out. The radiation is hardly attenuated, that is, the correction in bands 3 and 4 due to aerosols is low. The water vapor map shows a variable water vapor distribution. While above the ocean the value is mainly about 3.2 g*cm^{-2}, the water vapor column above the island of San Andrés is 4.11 g*cm^{-2}. This is a relatively high column, which means the band 8 should be corrected further because it is the absorption of the radiation of water vapor, the reflectances in band 8 in the corrected image. As is evident from the measurements of the Aerosol Robotic Network (AERONET) stations, the water vapor column — slightly higher on the surface — across the ocean and coastal waters were between 2.7 g*cm^{-2} and 3.7 g*cm^{-2}.

The separability analysis

To assess the separability of the atmospheric correction models in discriminating different land-covers (vegetation, coral rocks, soil, asphalt, sand, and deep water), we calculated it from the S2-A MSI corrected image. Then, we manually extracted the pixels of the composition of the different land-covers directly from the atmospheric correction models (ELM, SEN2COR, and ATCOR) imagery results. Finally, the separability analysis was performed, between the reflectance values TOA and BOA, for each of the spectral bands of the S2-A scene.

A separability index (Equation *3*) was used to estimate the effectiveness of the three models to discriminate the different class cover:

$$M = \frac{|\mu_b - \mu_u|}{\sigma_b + \sigma_u} \quad (3)$$

where μ_b and μ_u are the mean values of the considered difference of spectral separability of different land-cover types, and σ_b and σ_u are the corresponding standard deviations. The separability index has been frequently used to assess the degree of discrimination in remote sensing studies and imaging spectroscopy sensors (Meng et al., 2017), where the higher the separability value, the better the discrimination. A value of $M < 1$ denotes that the histograms overlap between the cover classes and the ability to separate the two-pixel groups is poor, while a value of $M > 1$ represents a good separability.

Results and discussion

The accuracy of the atmospheric correction models is determined by the statistic validation process through the resulting RMSE, standard deviation (SD), and the coefficient of determination (R^2), obtained from the 20% of the field data (eight validation targets), as a measure of how far estimates and forecasts values differ from real values.

The four wavebands scatterplots for the implementation of the ELM are shown in Figure 4. The regression line and confidence intervals are also shown and equations for each band, including the estimated regression coefficients and their associated coefficient of determination (R^2).

Figure 5 shows the endmembers of the four land-covers types extracted from the 32 calibration sites (coral rocks, asphalt, sand, and soil), which were chosen from their spectral homogeneity and invariant characteristics (Smith & Milton, 1999) of the archipelago.

A closer look at Figure 5 shows the differences between reflectance levels measures on the Sentinel

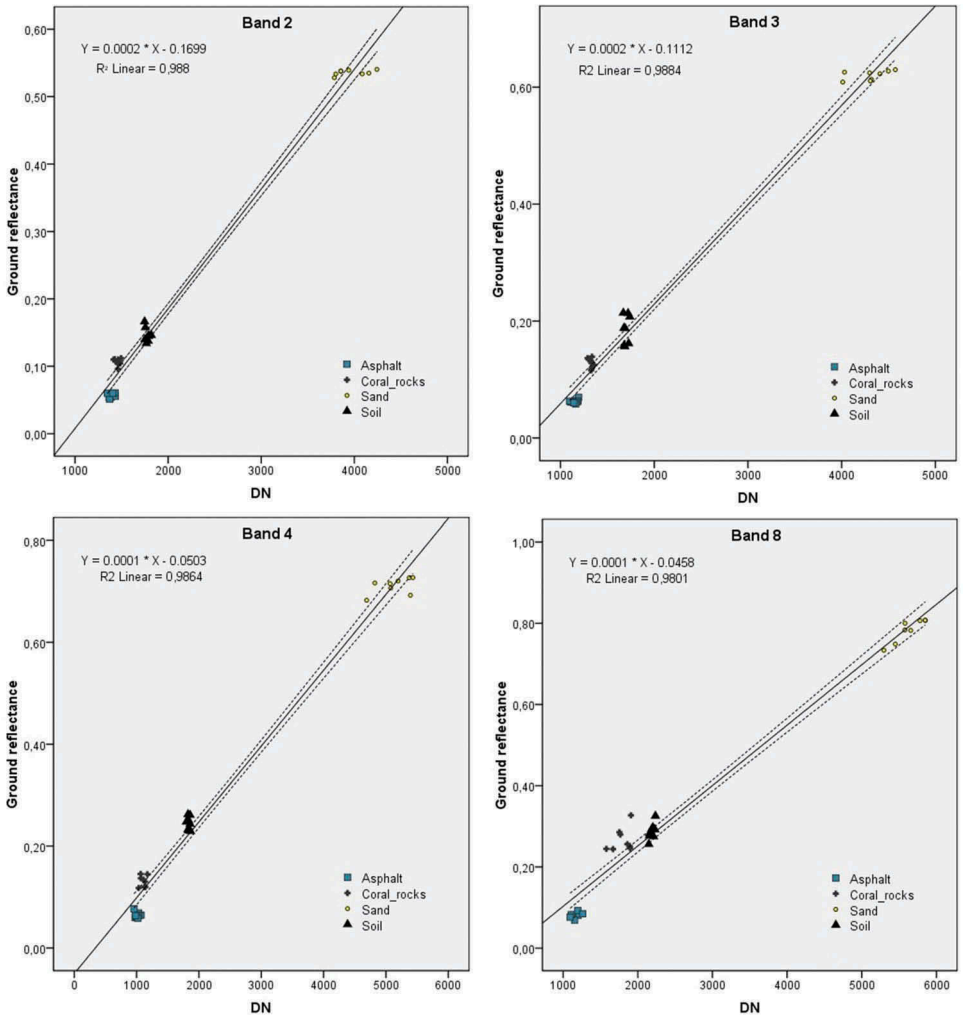

Figure 4. Scatterplots and regressions for at-ground reflectance against at-sensor radiance (DN).

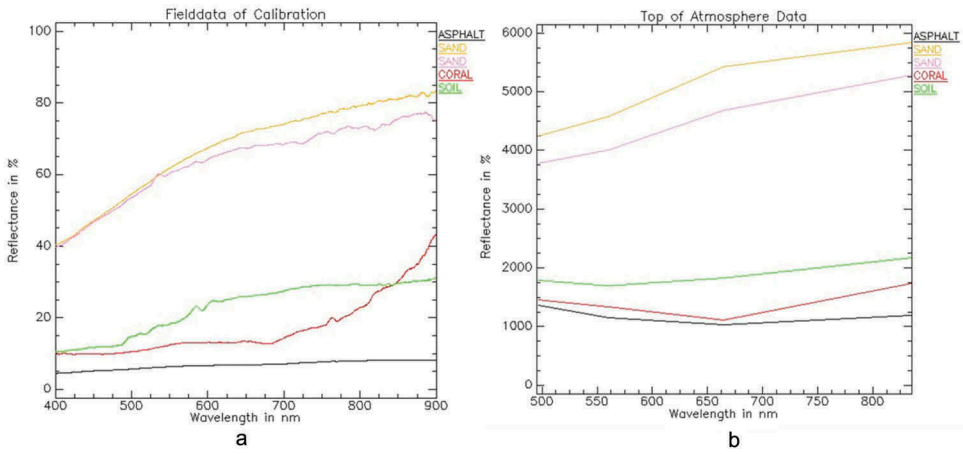

Figure 5. *In situ* measured reflectance spectrum (A) vs. TOA corrected SA-2 image (B) extracted spectrum for test sites.

SA-2 image and the real reflectance measured on the bottom of the atmosphere. TOA values recorded by the sensor were extracted from the image on pixels associated with each test site of calibration targets. These values in each band (2, 3, 4, and 8) were plotted against the corresponding ground reflectance for the calibration sites, and linear regression was used to derive a set of four prediction equations for the image, one for each waveband (Karpouzli & Malthus, 2003).

Validation of the BOA reflectance

We evaluate the performance of the model from eight validation test sites, its targets covering a wide range of

Table 3. Statistical summary of atmospheric correction results.

	ELM	SEN2COR	ATCOR
Average RMSE	0.0453	0.0777	0.0575
Standard Deviation	0.0193	0.0718	0.0358
Maximum RMSE	0.0604	0.1518	0.0913
Minimum RMSE	0.0235	0.0086	0.0200

reflectance values. Table 3 shows the statistical summary of the average RMSE error and standard deviation for each atmospheric correction model.

Figure 6 shows a box-plot of the average mean differences in spectral signatures after atmospheric correction at each of the eight sample validation sites for every atmospheric correction model. Visual analysis of the box-plot of RMSE values for each atmospheric correction approach shows that the ELM model slightly outperformed the other methodologies, while the SEN2COR calibration model provided the weakest estimates of reflectance measure. Mean difference in reflectance for the scene S2-A was around 0.0453, similar to those found in the validation works of Pflug, Main-Knorn, Makarau, and Richter (2015) in Central Europe. However, for Caribbean regions, this uncertainty is approximately below 21% for ATCOR and SEN2COR.

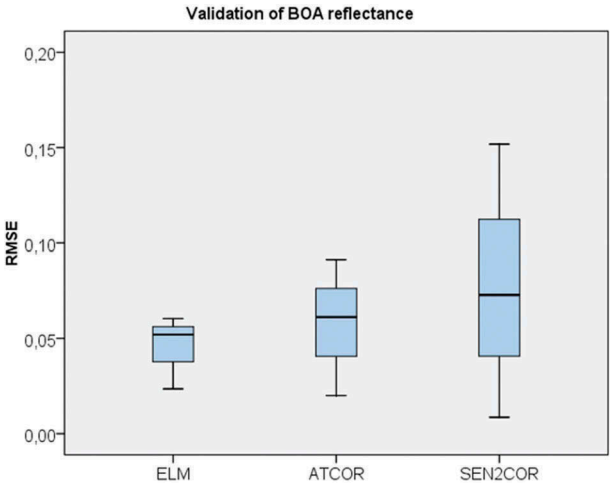

Figure 6. Mean differences in spectral signatures after atmospheric correction.

The ELM atmospheric correction technique was then applied to the Sentinel-2 satellite image dataset. This technique differs with respect to models (ATCOR or SEN2COR) inputs, computation efficiency, input data (e.g., raw brightness values or calibrated radiance) and required reference spectra (either *in situ* or from spectral libraries). However, in both cases, the resultant output is the same: scaled percent reflectance. Figure 7 shows the results of the atmospheric correction applied by the three models on the island of San Andrés. The coefficients of determination R^2 on the ELM model for the visible spectral region (458–680 nm) were all greater than 0.98, and for the NIR (785–900 nm) was 0.97. In general, the results show that the relationships found were near linear, with a better accuracy compared to calibration and validation results from others studies (Hadley et al., 2005); this is of significance because it supports a broader set of remote sensing applications

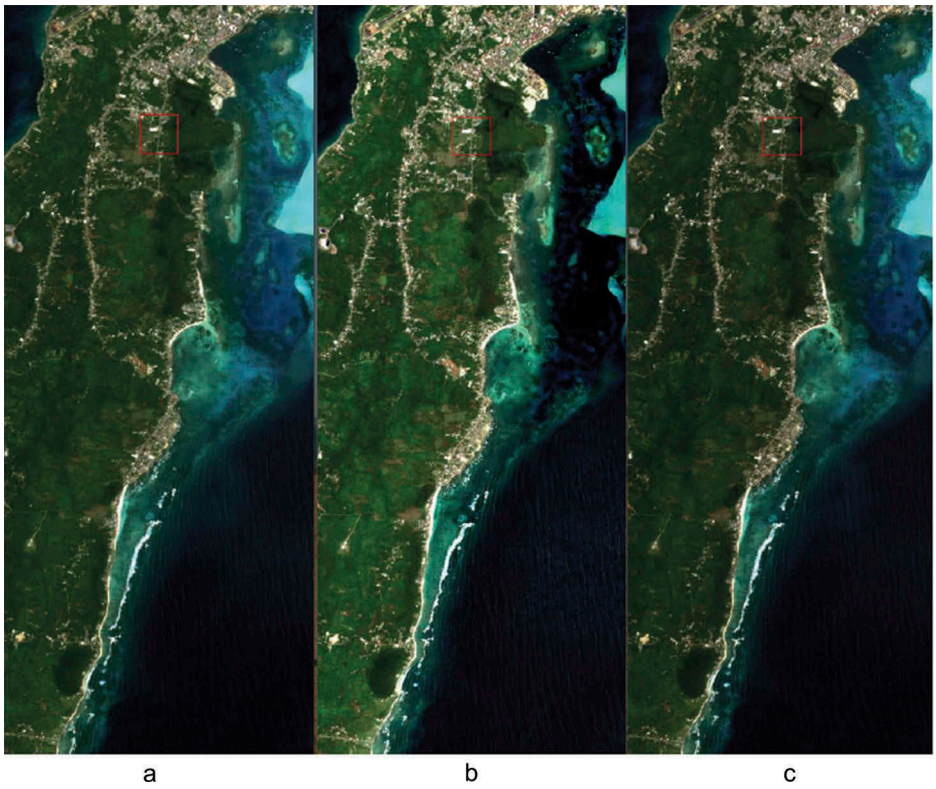

Figure 7. RGB composite of output image (Bottom of atmosphere): A) ELM B) ATCOR C) SEN2COR.

from better adjusted atmospheric correction models in tropical Caribbean zones.

The separability of the ELM model in discriminating land covers

The separability index (M) values for each model are listed in Table 4. The ATCOR model had the highest M value (9.134), followed by the ELM with 4.045 and SEN2COR with 3.469 for bare soil covers in the B2 (458–523 nm). For vegetation covers in the NIR (785–900 nm), the ELM model had the highest M value (M = 1,606), demonstrating high discriminatory power, followed by the SEN2COR and ATCOR (M = 0.728 and M = 0.671, respectively). This is consistent with the work of Vanonckelen et al. (2013), where their results showed that all corrected images resulted in higher overall classification accuracies than the uncorrected images. The highest accuracy for the full validation set was achieved after atmospheric correction. This approach demonstrates that the atmospheric correction of satellite images is necessary for many applications of remote sensing, that is, computation of vegetation indices and biomass estimation; additionally, due to the spatial and temporal variability of aerosol amount and type in tropical zones, it is crucial to be able to rely on accurately corrected satellite data.

The frequency distributions of the effect of atmospheric corrections (TOA and BOA) on a subset of image S2A for land-covers (without water) of the San Andrés Island are shown in four bands (Figure 8). These results show more consistency with spectral separability for different land-cover types: for example, the discrimination results on vegetation covers is a 15% higher in the ELM model. The histograms of TOA and BOA were well separated and relatively easy to

Table 4. M index values comparing ELM and other models separability for covers.

		Separability index values (M)					
Models	Band	Vegetation	Coral rocks	Sand	Asphalt	Soil	Deep Water
ELM	B2	2.653	1.149	1.307	0.254	4.045	0.195
	B3	0.528	0.136	1.879	0.025	0.496	0.061
	B4	0.052	0.554	1.670	0.140	0.559	0.590
	B8	1.606	1.884	3.176	0.440	1.427	1.074
SEN2COR	B2	1.970	0.712	1.200	0.180	3.469	0.141
	B3	0.412	0.195	1.456	0.000	0.304	0.000
	B4	0.289	0.177	1.026	0.050	0.093	0.090
	B8	0.728	0.737	1.585	0.147	0.556	0.048
ATCOR	B2	2.244	1.663	3.346	0.910	9.134	0.559
	B3	0.706	0.209	3.414	0.477	0.952	0.296
	B4	0.768	0.287	2.845	0.208	0.019	0.500
	B8	0.671	0.604	2.642	0.210	0.729	0.255

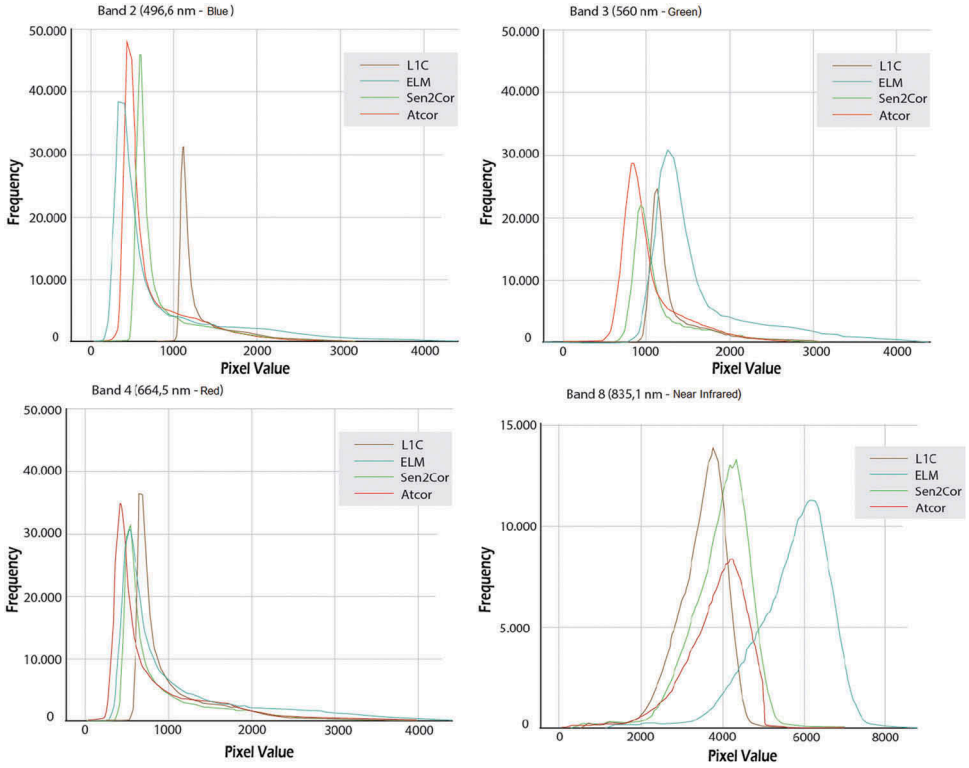

Figure 8. Comparison of atmospheric correction models on land-covers in San Andres Island, in the bands 2. 3 .4 and 8 of SA-2 MSI.

discriminate in the ELM model (M = 2.653) and ATCOR (M = 2.244), respectively. On the other hand, in the SEN2COR model, the spectral separability values on bare soil and sand covers had a higher value (M = 9.134, M = 3.346, respectively), discriminated on the NIR band compared with the values of other land-covers.

A comparison of the histograms of corrected images (Figure 8) showed that ELM and ATCOR had similar results; however, the SEN2COR model produces reflectance values closer to surface reflectance in the BOA scene, which can also be observed in the subset scene of the island surface. These results would suggest that in the SEN2COR model, the Rayleigh scattering over maritime areas was slightly sub-estimated, while ATCOR produces betters results; nonetheless, additional research is necessary to demonstrate this.

The band 3 (543–578 nm) and 4 (650–680 nm) of S2-A are well corrected with SEN2COR in the total scene, while for ATCOR the correction is slightly lower. From a closer examination of the correction parameters of the models, it was found that the AOT values where different for ATCOR and SEN2COR (Müller-Wilm, 2016), which lead to different results in the corrected images, especially in the band 8 (NIR) where the differences between ELM data and ATCOR and SEN2COR data are underestimated; on the other hand, the ELM data show reflectance more strongly than the other models. This observation suggests that ATCOR and SEN2COR highly underestimated the real value of the water vapor column, and therefore, the wavelengths in the region of the near infrared (785–900 nm) have weaker reflection values. However, in order to validate this affirmation, additional research and the use of secondary data like AERONET stations, also, is necessary to analyze the effects of other aerosol types for the correction parameters.

Band ratios and NDVI

In the differential images (Figure 9), the data for each band from the TOA and the ELM-BOA data, the atmospheric influence is recognizable. In the band 2, the radiation in the TOA image was increased due to Rayleigh scattering, the difference of the reflectance being about 7% or more, band 3 and band 4 show only slight differences, while in the near infrared, a strong increase in TOA reflectivity can be seen. This is an average of 10% to 20% with a few peaks around the 30%. Significant exceptions are water and asphalt (runway of the airport); in these areas, the difference between TOA and BOA is very small and thus stands in stark contrast to the other land-covers. This is made possible by the object-dependent, very low reflectance in the NIR region. In the formation of the ELM, TOA image in the NIR band increases linearly, and the difference between the absolute reflections is therefore always still in the low range.

The NDVI is based on the contrast between reflecting radiation in the red (543–578 nm) spectral range and in NIR (650–680 nm); therefore, if the contrast increases, the index also increases. The comparison of NDVI images clearly shows the correction of atmospheric effects because wavelengths in the region of the near infrared before the atmospheric correction by water vapor are absorbed, so after the correction, there can be an increase in the reflection. In the area of the red spectral range, the reflection of wavelengths was somewhat reduced by the correction (see AOT, Müller-Wilm, 2016), while before the correction, the increase from R to NIR is small, it increases after the correction. This effect produces NDVI values that vary up to 13% after the correction (Figure 10), compared to the values observed in the validation (Table 5).

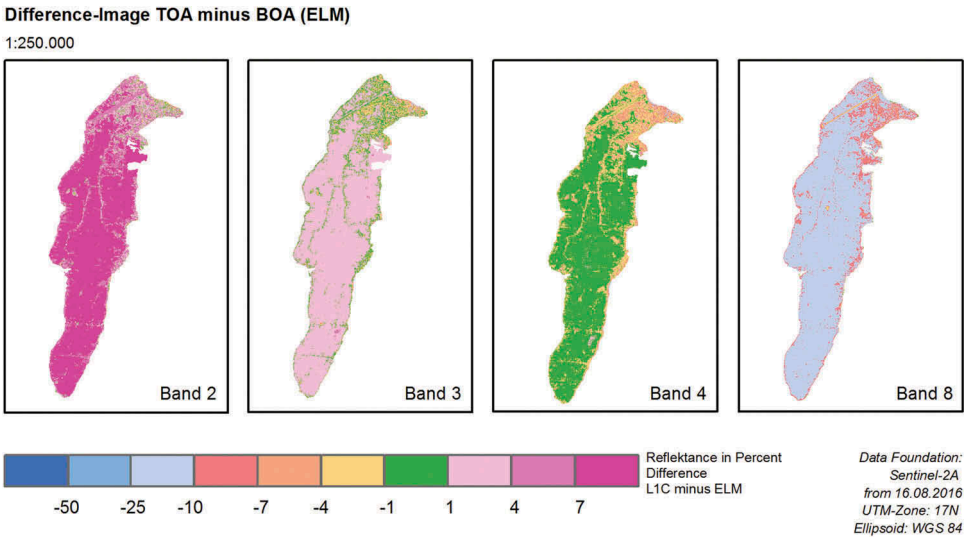

Figure 9. Differential images between TOA and BOA reflectance, comparison of spectral bands.

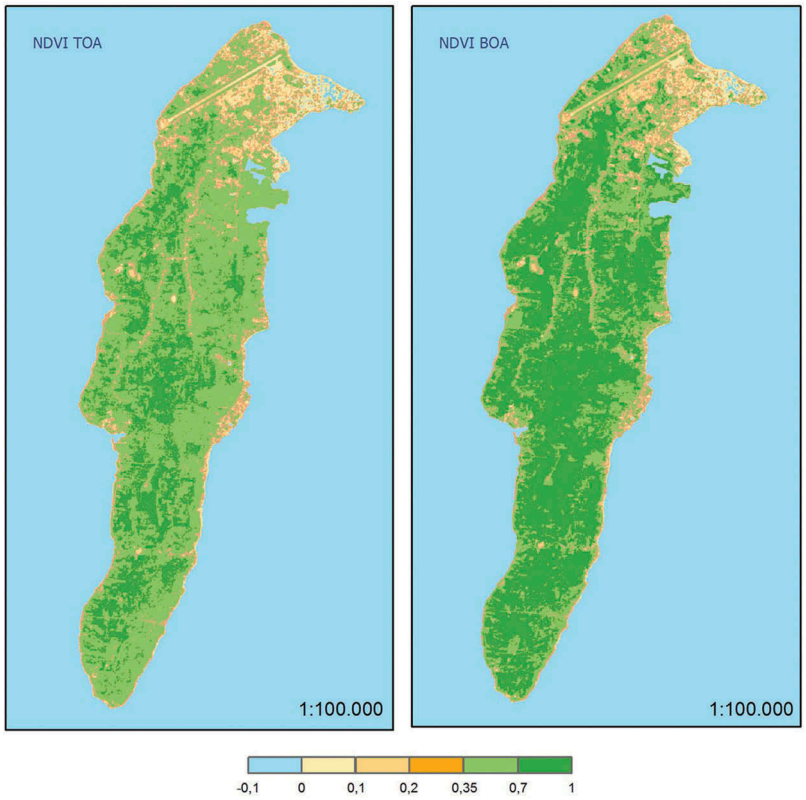

Figure 10. Display of the NDVI before and after the correction of atmospheric interferences on satellite image Sentinel 2-A.

Table 5. Comparison of the validation of NDVI means values Sentinel 2A, after atmospheric correction.

	TOA — L1C Reflectance	BOA — ELM Reflectance
NDVI (*Mean observed)	0.555	0.635
Difference (Field data)	0.094	0.013

*The mean value is calculated on 10 observations of vegetation in the field.

Conclusions

The results of this study have shown that the use of the empirical linear method or ELM in atmospheric correction is a simple method and effective methodology for calibrating remotely sensed data to units of ground reflectance. Although the validation and calibration targets used in the study were selected from a broad spectrum, it is necessary to identify all the variety of spectra present in the image in order to obtain more accurate values of the ground reflectance (BOA) on different land-cover types. However, the ELM has a large correlation coefficient observed between reflectance values of MSI sensor and ground reflectance for the four Sentinel 2A wavebands (2, 3, 4, and 8), and the calibration process as well as independent error assessment demonstrates that the ELM can be applied to correct Sentinel 2A imagery with highly satisfactory results in tropical zones.

The increased spatial resolution present in Sentinel 2A images made it possible to identify homogeneous test sites that were sufficiently radiometry stable, an important parameter in the calibration process.

Some findings of our research show that after atmospheric correction, the vegetation areas in the ELM model presented a better spectral separability, with 30–35% more than in the SEN2COR model in the blue band, and 85–95% in the NIR band, allowing better adjustments in the estimation of the spectral NDVI index, which makes it possible to deduce that the ground reflectance value seemed to play a more significant role in estimating the percentage of vegetation at the pixel level. On the other hand, the sand zones were spectrally closer to coral rocks in the NIR band in the ELM model, whereas the same areas were 45–55% better separated through the ATCOR model than other models.

To guide future applications of this methodology, it is essential to provide calibration and validation results as well as an estimate of the errors encountered. Further development of the methodology will require consideration of the bi-directional reflectance (BDRF) properties of the targets, as even coral rocks may exhibit reflectance anisotropy due to surface topography and measurement of the spatial variability of the atmospheric path radiance throughout the image or the adjacent reflectance from other areas of interest.

Acknowledgments

We sincerely thank the Centre for Oceanographic and Hydrographic Research of Colombia (CIOH) for providing

data from the San Andrés Archipelago, the European Space Agency (ESA) for providing Sentinel data, and the Validation Team for gathering feedback and exchanging ideas. We thank the IGAC-CIAF and their staff for providing its laboratories and supplying the spectroradiometry equipment used in this investigation.

Disclosure statement

No potential conflict of interest was reported by the authors.

References

Berk, A., Bernstein, L.S., Anderson, G.P., Acharya, P.K., Robertson, D.C., Chetwynd, J.H., & Adler-Golden, S.M. (1998). MODTRAN cloud and multiple scattering upgrades with application to AVIRIS. *Remote Sensing of Environment*, *65*, 367–375.

Drusch, M., Del Bello, U., Carlier, S., Colin, O., Fernandez, V., Gascon, F., … Bargellini, P. (2012). Sentinel-2: ESA's optical high-resolution mission for GMES operational services. *Remote Sensing of Environment*, *120*, 25–36.

Ferrier, G., & Trahair, N.S. (1995). Evaluation of apparent surface reflectance estimation methodologies. *International Journal of Remote Sensing*, *16*, 2291–2297.

Gao, B.-C., Montes, M.J., Davis, C.O., & Goetz, A.F.H. (2009). Atmospheric correction algorithms for hyperspectral remote sensing data of land and ocean. *Remote Sensing of Environment*, *113*, S17–S24.

Gilabert, M.A., Conese, C., & Maselli, F. (1994). An atmospheric correction method for the automatic retrieval of surface reflectances from TM images. *International Journal of Remote Sensing*, *15*, 2065–2086.

Goyens, C., Jamet, C., & Schroeder, T. (2013). Evaluation of four atmospheric correction algorithms for MODIS-Aqua images over contrasted coastal waters. *Remote Sensing of Environment*, *131*, 63–75.

Hadley, B.C., Garcia-Quijano, M., Jensen, J.R., & Tullis, J. A. (2005). Empirical versus model-based atmospheric correction of digital airborne imaging spectrometer hyperspectral data. *Geocarto International*, *20*, 21–28.

Karpouzli, E., & Malthus, T. (2003). The empirical line method for the atmospheric correction of IKONOS imagery. *International Journal of Remote Sensing*, *24*, 1143–1150.

Kneizys, F.X., Anderson, G.P., Shettle, E.P., Gallery, W.O., Abreu, L.W., Selby, J.E.A., … Clough, S.A. (1988) User's Guide to LOWTRAN-7. http://www.dtic.mil/dtic/tr/fulltext/u2/a206773.pdf.

Kobayashi, S., & Sanga-Ngoie, K. (2008). The integrated radiometric correction of optical remote sensing imageries. *International Journal of Remote Sensing*, *29*, 5957–5985.

Liang, S., & Fang, H. (2004). An improved atmospheric correction algorithm for hyperspectral remotely sensed Imagery. *IEEE Geoscience and Remote Sensing Letters*, *1*, 112–117.

Matthew, M.W., Adler-Golden, S.M., Berk, A., Felde, G., Anderson, G.P., Gorodetzky, D., … Shippert, M. (2003) Atmospheric correction of spectral imagery: Evaluation of the FLAASH algorithm with AVIRIS data. *SPIE Proceeding*. http://spectral.com/pdf/Atmospheric_Correction_of_Spectral.pdf.

Meng, R., Wu, J., Schwager, K.L., Zhao, F., Dennison, P.E., Cook, B.D., … Serbin, S.P. (2017). Using high spatial resolution satellite imagery to map forest burn severity across spatial scales in a Pine Barrens ecosystem. *Remote Sensing of Environment*, *191*, 95–109.

Minomura, M., Kuze, H., & Takeuchi, N. (2001). Adjacency effect in the atmospheric correction of satellite remote sensing data: Evaluation of the influence of aerosol extinction profiles. *Optical Review*, *8*, 133–141.

Moran, M.S., Jackson, R.D., Slater, P.N., & Teillet, P.M. (1992). Evaluation of simplified procedures for retrieval of land surface reflectance factors from satellite sensor output. *Remote Sensing of Environment*, *41*, 169–184.

Müller-Wilm, U. (2016) Sentinel-2 MSI – Level-2A Prototype Processor Installation and User Manual. http://step.esa.int/thirdparties/sen2cor/2.2.1/S2PAD-VEGA-SUM-0001-2.2.pdf.

Pflug, B., Main-Knorn, M., Makarau, A., & Richter, R. (2015). Validation of aerosol estimation in atmospheric correction algorithm ATCOR. *ISPRS - International Archives of the Photogrammetry, Remote Sensing and Spatial Information Sciences*, *XL-7/W3*, 677–683.

Psj, C. (1996). Image-based atmospheric corrections - revisited and improved. *Photogrammetric Engineering and Remote Sensing*, *62*, 1025–1036.

Rahman, H., & Dedieu, G. (1994). SMAC: A simplified method for the atmospheric correction of satellite measurements in the solar spectrum. *International Journal of Remote Sensing*, *15*, 123–143.

Richter, R. (1996). Atmospheric correction of satellite data with haze removal including a haze/clear transition region. *Computers & Geosciences*, *22*, 675–681.

Rouquié, B., Hagolle, O., Bréon, F.-M., Boucher, O., Desjardins, C., & Rémy, S. (2017). Using copernicus atmosphere monitoring service products to constrain the aerosol type in the atmospheric correction processor MAJA. *Remote Sensing*, *9*, 12.

Schläpfer, D., & Richter, R. (2017). *Atmospheric Correction Of Imaging Spectroscopy Data Using Shadow-based Quantification Of Aerosol Scattering Effects*, 21–28. doi:10.12760/01-2017-1-03.

Smith, G.M., & Milton, E.J. (1999). The use of the empirical line method to calibrate remotely sensed data to reflectance The use of the empirical line method to calibrate remotely sensed data to reflectance. *International Journal of Remote Sensing*, *20*, 2653–2662.

Sriwongsitanon, N., Surakit, K., & Thianpopirug, S. (2011). Influence of atmospheric correction and number of sampling points on the accuracy of water clarity assessment using remote sensing application. *Journal of Hydrology*, *401*, 203–220.

USGS (2017) USGS Spectroscopy Lab - home page. https://speclab.cr.usgs.gov/.

Vanonckelen, S., Lhermitte, S., & Van Rompaey, A. (2013). The effect of atmospheric and topographic correction methods on land cover classification accuracy. *International Journal of Applied Earth Observation and Geoinformation*, *24*, 9–21.

Werdell, P.J., Franz, B.A., & Bailey, S.W. (2010). Evaluation of shortwave infrared atmospheric correction for ocean color remote sensing of Chesapeake Bay. *Remote Sensing of Environment*, *114*, 2238–2247.